Fluid Flow and Heat Transfer in an Axially Rotating Pipe: The Rotational Entrance

B. WEIGAND and H. BEER
Institut für Technische Thermodynamik
Technische Hochschule Darmstadt
Petersenstrasse 30
6100 Darmstadt, Germany

ABSTRACT

The complex interactions between turbulence and rotation in the rotational entrance region of a pipe, rotating about its axis, are examined.
By assuming a universal tangential velocity profile and with the use of a modified mixing length theory, the development of the axial velocity profile and the heat transfer coefficient along the rotational entrance length are calculated. The theoretical results are compared with experimental findings of Reich [8].

1. INTRODUCTION

Fluid flow and heat transfer in rotating pipes are not only of considerable theoretical interest, but also of great practical importance. An obvious technical application is a rotating power transmission shaft that is longitudinally bored, and through which a fluid is pumped for cooling of turbine blades or for other purposes.
When a fluid enters a pipe rotating about its axis, tangential forces acting between the rotating pipe and the fluid cause the fluid to rotate with the pipe, resulting in a flow pattern which is rather different from that observed in a nonrotating pipe. Rotation was found to have a very marked influence on the suppression of the turbulent motion because of radially growing centrifugal forces.
In 1929 Levy [1] studied experimentally the flow in rotating pipes. Murakami and Kikuyama [2] measured the time-mean velocity components and hydraulic losses in an axially rotating pipe when a fully developed turbulent flow was introduced into the pipe. The pipe rotation was found to suppress the turbulence in the flow, and also to reduce the hydraulic loss. With increasing rotational speed the axial velocity distribution finally approaches the Hagen-Poiseuille flow. Kikuyama et al [3] calculated the velocity distribution in the fully developed region of a rotating pipe with the help of a modified mixing length theory proposed by Bradshaw [4]. They assumed the tangential velocity to be a parabolic distribution $v_\varphi/v_{\varphi w} = (r/R)^2$ in the fully developed region, which was well confirmed by experiments [2], [3].
Reich and Beer [5] examined experimentally and by analysis the effect of tube rotation on the velocity distribution and on the heat transfer to a fluid flowing inside a tube. The flow was thermaly and hydrodynamically fully developed. For their calculations they used a slightly different mixing length formula as proposed in [3]. With an increase in the rotation rate $N = v_{\varphi w}/\bar{v}_{z0}$ they observed a remarkable decrease in heat transfer. The experimental observations were in close agreement with their theory. The remarkable decrease in heat transfer with increasing N results from the

strong relaminarization caused by the centrifugal forces. For growing values of N, the effect of rotation becomes more pronounced and the Nusselt number approaches gradually the value for laminar pipe flow.
For a hydrodynamic fully developed flow the thermal entrance region was examined in [6]. The analytical investigation showed that the problem could be reduced to a Graetz-Problem. With increasing rotational Reynolds number Re_φ a remarkable decrease in heat transfer was observed. The thermal entrance length increases remarkably with growing Re_φ. For $Re_D = 50000$ and $N = 3$, the flow needs nearly 200 pipe diameters to get thermally fully developed.
The following study will focus attention on the fluid flow and heat transfer inside an axially rotating pipe in the combined hydrodynamic and thermal entrance region. Heretofore the interaction of centrifugal forces and turbulence was investigated only in the hydrodynamic rotational entrance by experiments [8], [16].

2. ANALYSIS

2.1 The Conservation Equations in Cylindrical Coordinates:

The problem under consideration is of great practical importance, because in most rotating machinery the geometric configurations are not large enough to guarantee fully developed flow conditions.
Because of steady flow conditions and cylindrical symmetry, there are no variations in time and in tangential direction. By assuming an incompressible, Newtonian fluid with constant fluid properties, the conservation equations for the time smoothed variables may be written as follows:

$$\frac{\partial v_r}{\partial r} + \frac{v_r}{r} + \frac{\partial v_z}{\partial z} = 0 \tag{1}$$

$$\frac{v_\varphi^2}{r} = \frac{1}{\rho}\frac{\partial p}{\partial r} \tag{2}$$

$$\rho\left[v_r \frac{\partial v_\varphi}{\partial r} + \frac{v_r v_\varphi}{r} + v_z \frac{\partial v_\varphi}{\partial z}\right] = \frac{1}{r^2}\frac{\partial}{\partial r}\left(r^2 \tau_{r\varphi}\right) \tag{3}$$

$$\rho\left[v_r \frac{\partial v_z}{\partial r} + v_z \frac{\partial v_z}{\partial z}\right] = -\frac{\partial p}{\partial z} + \frac{1}{r}\frac{\partial}{\partial r}\left(r\,\tau_{rz}\right) \tag{4}$$

$$\rho\, c_p\left[v_r \frac{\partial T}{\partial r} + v_z \frac{\partial T}{\partial z}\right] = -\frac{1}{r}\frac{\partial}{\partial r}\left(r\,\dot{q}_r\right) \tag{5}$$

By deriving the eqs. (2) - (5) the usual boundary-layer assumptions were made, which are a common treatment of the conservation equations for pipe flow [7], [14].
The components of the stress tensor, which appear in eqs. (3) and (4) can be written for a Newtonian fluid as follows

$$\tau_{r\varphi} = \mu\, r \frac{\partial}{\partial r}\left(\frac{v_\varphi}{r}\right) - \rho\,\overline{v_r' v_\varphi'} \tag{6}$$

$$\tau_{rz} = \mu \frac{\partial v_z}{\partial r} - \rho\,\overline{v_r' v_z'} \tag{7}$$

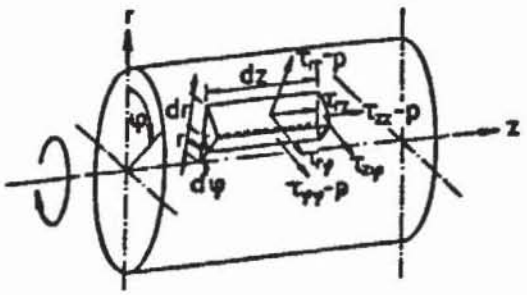

FIGURE 1. Cylindrical coordinate system

The coordinate system and the components of the stress tensor are illustrated in fig. 1. The radial component of the heat flux vector is:

$$\dot{q}_r = - k \frac{\partial T}{\partial r} + \rho c_p \overline{v_r' T'} \tag{8}$$

The parabolic nature of the boundary-layer equations requires that boundary conditions be provided on three sides of the solution domain. In addition to initial conditions for the momentum and energy equations, symmetry is assumed. At the pipe wall the heat flux is prescribed and the zero slip condition holds.

$$r = R : \quad v_r = 0 ; \quad v_\varphi = v_{\varphi W} ; \quad v_z = 0 ; \quad - k \frac{\partial T}{\partial r} = \dot{q}_{rW}$$

$$r = 0 : \quad v_r = 0 ; \quad v_\varphi = 0 \quad ; \quad \frac{\partial v_z}{\partial r} = 0 ; \qquad \frac{\partial T}{\partial r} = 0$$

$$z = 0 : \quad p = p_o ; \quad T = T_o \quad ; \quad v_z = h(r) \tag{9}$$

According to eq. (9) it is assumed that the fluid enters the rotating pipe section with a fully developed, turbulent velocity profile. This initial condition was chosen to compare results with measurements of Reich [8].

2.2 The Universal Tangential Velocity Distribution

Fig. 2 shows experimental tangential velocity profiles for various z/D and different values of the rotation rate N. It is obvious, that the profiles are only slightly or not at all influenced by the flow-rate Reynolds number and by N.

This fact was also recognized in [8] and [9]. Increasing rotational Reynolds numbers results in a growing shear stress in the tangential direction which leads to an only slight dependence of the tangential velocity profile on N. This will influence the entrance length which is needed for the development of the tangential velocity profile. Therefore, it is reasonable to introduce a quite universal profile to describe the tangential velocity distribution:

$$\frac{v_\varphi}{v_{\varphi W}} = \tilde{r}(2 + f(\tilde{z})) \tag{10}$$

$$f(\tilde{z}) = \frac{1}{\tilde{z}} + 9.5 \, e^{-0.019 \, \tilde{z}} \tag{11}$$

with $\tilde{r} = r/R$ and $\tilde{z} = z/R$.

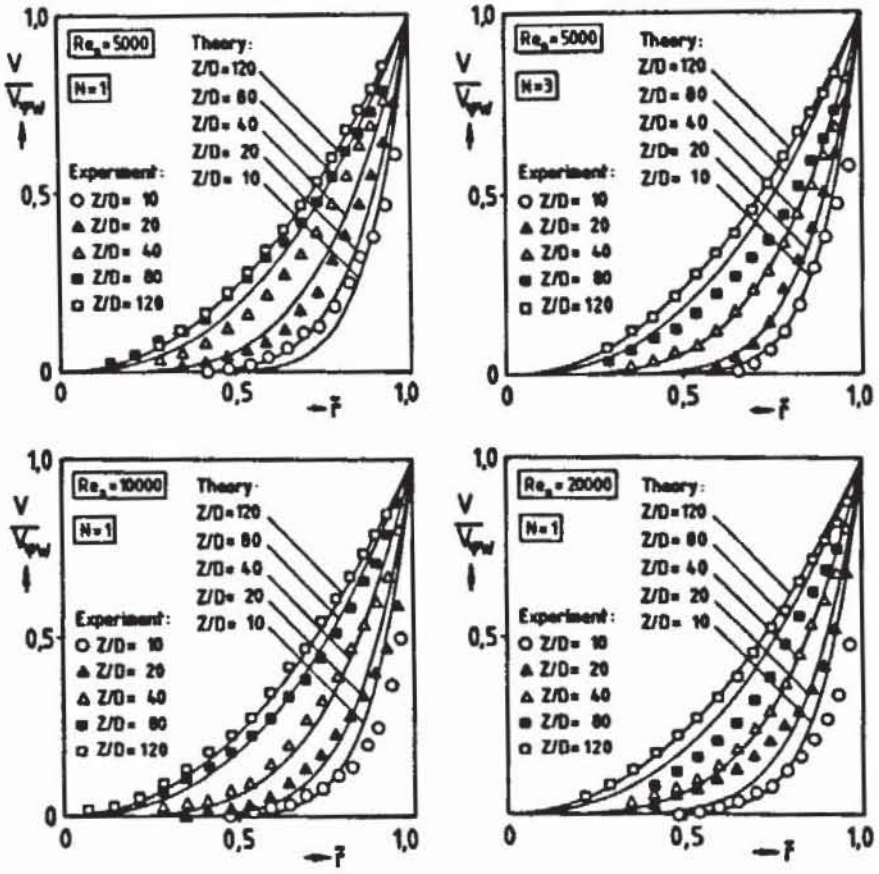

FIGURE 2. Tangential velocity distribution as a function of the axial coordinate z/D.

The universal tangential velocity profile is assumed to be only a function of the rotational length. Fig. 2 shows that this assumption is well confirmed by experiments [8], which were performed with air. Because the tangential velocity distribution is now given by eq. (10) and the pressure is not a function of the tangential coordinate, eq. (3) can be omited.
However, it has to be pointed out that an extrapolation of eq. (10) to $N > 3$ is admissible only if experimental findings which confirm the universality of eq. (10) for larger values of N were available.

2.3 The Turbulence Model

In order to find a solution of the differential equations (1) -(5) with the boundary conditions (9), a relation between the Reynolds shear stresses and the time mean velocity components must be established. This will be done by the use of a mixing length hypothesis proposed by Koosinlin [10]. This turbulence model is well confirmed for fluid flow and heat transfer in rotating pipes [3], [5], [6]. It has to be pointed out, that such a simple turbulence model can be used sucessfully only, if the tangential velocity profile is known. Without knowledge of the tangential velocity distribution the laminarization phenomena can only be calculated applying the stress equations turbulence model, which was shown by Hirai et al. [11] for fully developed flow conditions.
Using a modified Prandtl's mixing length theory, as proposed by Koosinlin

[10], the axial shear stess τ_{rz} in eq. (7) can be written as

$$\tau_{rz} = \left[\mu + \rho\, l^2 \left(\left[\frac{\partial v_z}{\partial r} \right]^2 + \left[r \frac{\partial}{\partial r} \left(\frac{v_\varphi}{r} \right) \right]^2 \right)^{1/2} \right] \frac{\partial v_z}{\partial r} \tag{12}$$

where l is the hydrodynamic mixing length.
The radial component of the heat flux vector eq. (8) is found to be

$$\dot{q}_r = \left[- k - \rho\, c_p\, l\, l_q \left(\left[\frac{\partial v_z}{\partial r} \right]^2 + \left[r \frac{\partial}{\partial r} \left(\frac{v_\varphi}{r} \right) \right]^2 \right)^{1/2} \right] \frac{\partial T}{\partial r} \tag{13}$$

where l_q denotes the thermal mixing length.
In a rotating system the turbulence, i.e. the mixing length l and l_q are markedly effected by the centrifugal forces [8], [9]. To describe the suppression of turbulence with radially growing centrifugal forces, the mixing length l_o of a nonrotating pipe must be modified for the flow in a rotating tube. Bradshaw [4] proposed the following equation:

$$\frac{l}{l_o} = (1 - \beta\, Ri)^\alpha \tag{14}$$

where α is a constant ($\alpha = 2$ used in [5]).
The Richardson number Ri appearing in eq. (14) describes the effect of tube rotation on turbulence. Ri is defined by

$$Ri = \frac{2 \frac{v_\varphi}{r^2} \frac{\partial}{\partial r} (v_\varphi\, r)}{\left[\frac{\partial v_z}{\partial r} \right]^2 + \left[r \frac{\partial}{\partial r} \left(\frac{v_\varphi}{r} \right) \right]^2} \tag{15}$$

Without rotation, Ri = 0, there exists a fully turbulent pipe flow. If Ri > 0, i.e. for a rotating tube with a radially growing tangential velocity, the centrifugal forces suppress the turbulent fluctuations and the mixing length decreases. If Ri < 0, e.g. for flows over spinning surfaces, the turbulence will be enhanced by rotation.
The function β in eq. (14) is a constant for fully developed flow, as it was shown in [5] by checking the boundary value of Ri for $N \to \infty$, which means the existence of quasi laminar flow for large N. This results in $\beta = 1/6$. In the case of hydrodynamically developing flow, the same procedure yields an expression for β, that is given by

$$\beta(\bar{z}) = \frac{(1 + f(\bar{z}))^2}{6 + 2f(\bar{z})} \quad , \quad N \to \infty \tag{16}$$

Of course, the value of $\beta(\bar{z})$ according to eq. (16) can only present an

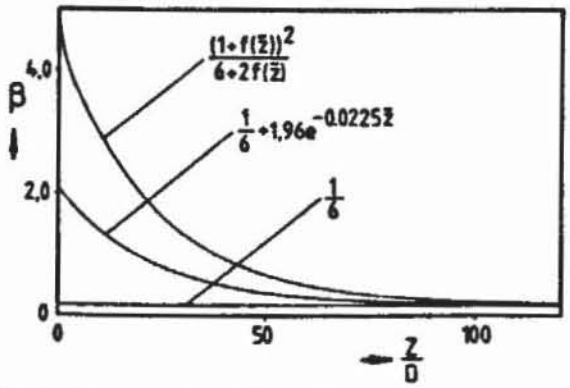

FIGURE 3. Function β

upper limit, pretending a fully laminar flow in a near wall region for large values of N. This will overpredict the laminarization phenomena in the rotational entrance region, because it ignores any interaction between the laminar wall region and the fully turbulent pipe flow in the central core, which is not yet effected by the radially growing centrifugal forces (fig. 2). Only for large values of z/D, if the centrifugal forces influence the whole cross sectional area of the tube, there must be a transition to a laminar like profile for $N \to \infty$. This means that $\beta(\tilde{z})$ must take values between 1/6 and that of eq. (16) for finite values of z/D. In order to overcome the above mentioned difficulties, a simple empirical expression for $\beta(\tilde{z})$ was developed, which is

$$\beta(\tilde{z}) = \frac{1}{6} + 1.96\, e^{-0.0225\,\tilde{z}} \tag{17}$$

Fig. 3 shows a comparison of $\beta(\tilde{z})$ according to eq. (16) and to eq. (17), respectively.

A common correlation between the mixing length in a nonrotating pipe l_o and the radial coordinate r is Nikuradse's mixing length expression [12], which is multiplied by the van Driest damping factor, in order to describe the disappearance of the mixing length near the tube wall, in the viscous sublayer.

$$\frac{l_o}{R} = \left[1 - e^{-y^+/26} \right] \left[0.14 - 0.08 \left(\frac{r}{R} \right)^2 - 0.06 \left(\frac{r}{R} \right)^4 \right] \tag{18}$$

with the dimensionless distance from the wall

$$y^+ = \frac{v_* (R - r)}{\nu} \tag{19}$$

and the friction velocity

$$v_* = \sqrt{\frac{|\tau_{rz}(r = R)|}{\rho}} \tag{20}$$

The influence of the centrifugal forces on the thermal mixing length is expressed by the same equation as the influence on the hydrodynamic mixing length.

$$\frac{l_q}{l_{qo}} = (1 - \xi\, Ri)^2 \tag{21}$$

where l_{qo} is the thermal mixing length for a nonrotating pipe which can be expressed by the turbulent Prandtl-number [12] as

$$\frac{1}{Pr_t} = \frac{l_{qo}}{l_o} = 1.53 - 2.82\, \tilde{r}^2 + 3.85\, \tilde{r}^3 - 1.48\, \tilde{r}^4 \tag{22}$$

according to experiments performed by Ludwieg [13] for air (Pr = 0.71).

2.4 The Dimensionless Equations

In eq. (2) the radial pressure gradient is balanced by the radially growing tangential velocity, which results in a radially increasing pressure difference. The maximum of the radial pressure difference between pipe wall and center will be attained for a fully developed tangential velocity profile. Reich showed [8] that this pressure difference is negligible for

airflow. Therefore, the pressure was assumed to be constant over the pipe cross section.
Introducing the following dimensionless quantities

$$\tilde{v}_z = v_z / \bar{v}_{z0} \quad , \quad \tilde{v}_\varphi = v_\varphi / \bar{v}_{z0}$$

$$\tilde{v}_r = \frac{v_r}{\bar{v}_{z0}} \sqrt{Re_R} \quad , \quad \tilde{v}_y = \frac{v_y}{\bar{v}_{z0}} \sqrt{Re_R}$$

$$\tilde{r} = r/R \quad , \quad \tilde{y} = \frac{R - r}{R} \sqrt{Re_R} \quad , \quad \tilde{z} = z/R$$

$$\theta = \frac{T_o - T}{\dot{q}_{rw} R} \frac{\lambda}{\sqrt{Re_R}} + 1 \quad , \quad \tilde{p} = \frac{p - p_o}{\rho \bar{v}_{z0}^2}$$

$$Re_R = \frac{\bar{v}_{z0} R}{\nu} \quad , \quad Pr = \frac{\nu}{a} \quad , \quad Re_\varphi = \frac{v_{\varphi W} R}{\nu} \quad , \quad N = \frac{v_{\varphi W}}{\bar{v}_{z0}} \tag{23}$$

into the eqs. (1), (2) - (5), results in the following differential equations

$$\frac{\partial}{\partial \tilde{y}} \left[\tilde{v}_y \tilde{r} \right] + \frac{\partial}{\partial \tilde{z}} \left[\tilde{v}_z \tilde{r} \right] = 0 \tag{24}$$

$$\tilde{v}_y \frac{\partial \tilde{v}_z}{\partial \tilde{y}} + \tilde{v}_z \frac{\partial \tilde{v}_z}{\partial \tilde{z}} = - \frac{\partial \tilde{p}}{\partial \tilde{z}} + \frac{1}{\tilde{r}} \frac{\partial}{\partial \tilde{y}} \left[\tilde{r} \left(1 + \varepsilon_m^+ \right) \frac{\partial \tilde{v}_z}{\partial \tilde{y}} \right] \tag{25}$$

$$\tilde{v}_y \frac{\partial \theta}{\partial \tilde{y}} + \tilde{v}_z \frac{\partial \theta}{\partial \tilde{z}} = \frac{1}{Pr} \frac{1}{\tilde{r}} \frac{\partial}{\partial \tilde{y}} \left[\tilde{r} \left(1 + \frac{Pr}{Pr_t} \varepsilon_m^+ \right) \frac{\partial \theta}{\partial \tilde{y}} \right] \tag{26}$$

with ε_m^+ defined by

$$\varepsilon_m^+ = \left(Re_R \right)^{3/2} \left(\frac{1}{\tilde{R}} \right)^2 \left[\left(\frac{\partial \tilde{v}_z}{\partial \tilde{y}} \right)^2 + \left(\tilde{r} \frac{\partial}{\partial \tilde{y}} \left[\frac{\tilde{v}_\varphi}{\tilde{r}} \right] \right)^2 \right]^{1/2} \tag{27}$$

Inserting the dimensionless quantities into the boundary conditions eq. (9) yields:

$$\tilde{y} = 0 \quad : \tilde{v}_y = 0 \; ; \; \tilde{v}_z = 0 \; ; \; \frac{\partial \theta}{\partial \tilde{y}} = - 1$$

$$\tilde{y} = \sqrt{Re_R} : \tilde{v}_y = 0 \; ; \; \frac{\partial \tilde{v}_z}{\partial \tilde{y}} = 0 \; ; \; \frac{\partial \theta}{\partial \tilde{y}} = 0$$

$$\tilde{z} = 0 \quad : \tilde{p} = 0 \; ; \quad \theta = 1 \; ; \; \tilde{v}_z = \tilde{h}(\tilde{r}) \tag{28}$$

In order to make eqs. (24) - (27) accesible to a numerical analysis and to ensure that the equations have a form that is common to plane and axisymmetric flow, the Mangler transformation [14] is applied:

$$d\bar{z} = d\tilde{z} \quad , \quad d\bar{y} = \tilde{r} \, d\tilde{y} \tag{29}$$

This results in

$$\frac{\partial \bar{v}_z}{\partial \bar{z}} + \frac{\partial \bar{v}_y}{\partial \bar{y}} = 0 \tag{30}$$

$$\bar{v}_z \frac{\partial \bar{v}_z}{\partial \bar{z}} + \bar{v}_y \frac{\partial \bar{v}_z}{\partial \bar{y}} = - \frac{\partial \bar{p}}{\partial \bar{z}} + \frac{\partial}{\partial \bar{y}} \left(b_1 \frac{\partial \bar{v}_z}{\partial \bar{y}} \right) \tag{31}$$

$$\bar{V}_z \frac{\partial \theta}{\partial \bar{z}} + \bar{V}_y \frac{\partial \theta}{\partial \bar{y}} = \frac{1}{Pr} \frac{\partial}{\partial \bar{y}} \left(b_2 \frac{\partial \theta}{\partial \bar{y}} \right) \tag{32}$$

with the following quantities

$$\bar{V}_z = \tilde{v}_z \quad , \quad \bar{V}_y = \tilde{r}\, \tilde{v}_y \quad , \quad \bar{p} = \tilde{p}$$

$$b_1 = \tilde{r}^2 (1+\varepsilon_m^+) \quad , \quad b_2 = \tilde{r}^2 \left(1+Pr/Pr_t\, \varepsilon_m^+\right)$$

Introducing the stream function, defined as

$$\bar{V}_z = \frac{\partial \bar{F}}{\partial \bar{y}} \quad , \quad \bar{V}_y = - \frac{\partial \bar{F}}{\partial \bar{z}} \tag{33}$$

eqs. (30) - (32) may be written as

$$\frac{\partial}{\partial \bar{y}} \left(b_1 \frac{\partial^2 \bar{F}}{\partial \bar{y}^2} \right) = \frac{\partial \bar{p}}{\partial \bar{z}} + \frac{\partial \bar{F}}{\partial \bar{y}} \frac{\partial^2 \bar{F}}{\partial \bar{z} \partial \bar{y}} - \frac{\partial^2 \bar{F}}{\partial \bar{y}^2} \frac{\partial \bar{F}}{\partial \bar{z}} \tag{34}$$

$$\frac{\partial}{\partial \bar{y}} \left(b_2 \frac{\partial \theta}{\partial \bar{y}} \right) = Pr \left(\frac{\partial \bar{F}}{\partial \bar{y}} \frac{\partial \theta}{\partial \bar{z}} - \frac{\partial \theta}{\partial \bar{y}} \frac{\partial \bar{F}}{\partial \bar{z}} \right) \tag{35}$$

The presence of $\partial \bar{p}/\partial z$ in eq. (34) introduces an additional unknown to the system given by eq. (34) and (35). Thus another equation is needed and is provided by the conservation of mass in integral form [14].

$$\bar{V}_{z_0} R^2 = 2 \int_0^R v_z\, r\, dr \quad \rightarrow \quad \frac{1}{2} \sqrt{Re_R} = F(\bar{y}_L) \tag{36}$$

with $\bar{y}_L = \frac{1}{2} \sqrt{Re_R}$.

At the centerline, symmetry requires $\partial v_z/\partial r$ and $\partial T/\partial r$ to be zero in untransformed coordinates. In terms of dimensionless variables the parameters $\partial \bar{V}_z/\partial \bar{y}$ and $\partial \theta/\partial \bar{y}$ at the centerline are indeterminate. Therefore, the boundary conditons at the centerline were calculated from eqs. (34) and (35), according to [15].
The boundary conditions are:

$$\bar{y} = 0 \; : \; \bar{F} = 0 \; ; \; \frac{\partial \bar{F}}{\partial \bar{y}} = 0 \; ; \; \frac{\partial \theta}{\partial \bar{y}} = -1$$

$$\bar{y} = \bar{y}_L \; : \; \frac{\partial^2 \bar{F}}{\partial \bar{y}^2} = - \frac{\sqrt{Re_R}}{2} \left[\frac{\partial \bar{p}}{\partial \bar{z}} + \frac{1}{2} \frac{\partial}{\partial \bar{z}} \left(\frac{\partial \bar{F}}{\partial \bar{y}} \right)^2 \right]$$

$$\frac{\partial \theta}{\partial \bar{y}} = - \frac{\sqrt{Re_R}}{2} Pr \frac{\partial \bar{F}}{\partial \bar{y}} \frac{\partial \theta}{\partial \bar{z}}$$

$$\bar{z} = 0 \; : \; \bar{p} = 0 \; ; \; \theta = 1 \; ; \; \bar{F} = \text{given} \tag{37}$$

2.5 The Numerical Method

In order to obtain solutions of eq. (34) and (35) with the boundary conditions eq. (37), an implicit finite-difference method is applied, which is known in literature as the Keller-box method. A detailed description can be found in [14] and [15]. Because the box scheme is a common method to solve parabolic differential equations, only a brief outline is provided here.

In consequence of the assumption of an incompressible fluid with constant properties, the equation of motion and the energy equation are uncoupled and may be solved separately.

The velocity distribution. The momentum eq. (34) will be first reduced to a first-order system of differential equations

$$F' = U \tag{38}$$

$$U' = V \tag{39}$$

$$\left(b_1 V\right)' = \frac{\partial \bar{P}}{\partial \bar{z}} + U \frac{\partial U}{\partial \bar{z}} - V \frac{\partial F}{\partial \bar{z}} \tag{40}$$

where primes denote differentiation with respect to $\bar{y}$. The following boundary conditions belong to eqs. (38) - (40)

$$\bar{y} = 0 \; : \; F = U = 0$$

$$\bar{y} = y_L \; : \; F = \frac{1}{2}\sqrt{Re_R} \quad , \quad V = -\frac{1}{2}\sqrt{Re_R}\left[\frac{\partial \bar{P}}{\partial \bar{z}} + \frac{1}{2}\frac{\partial}{\partial \bar{z}}(U^2)\right] \tag{41}$$

For $0 < \bar{z} < z_N$, $0 < \bar{y} < y_L$, a possibly nonuniform net is placed:

$$\bar{z}_o = 0 \qquad \bar{z}_n = \bar{z}_{n-1} + k_n \quad , \quad n = 1,2,\ldots,N \tag{42}$$

$$\bar{y}_o = 0 \qquad \bar{y}_j = \bar{y}_{j-1} + h_j \quad , \quad j = 1,2,\ldots,J, \; \bar{y}_J = \bar{y}_L$$

with k_n and h_j denoting variable distances between nodes in the $\bar{z}$ and $\bar{y}$ direction.
Eqs. (38) and (39) were approximated by central-difference quotients and averages about the midpoint $(\bar{z}_n, \bar{y}_{j-\frac{1}{2}})$, while eq. (40) was centered about the midpoint $(\bar{z}_{n-\frac{1}{2}}, \bar{y}_{j-\frac{1}{2}})$. After approximating the boundary conditions, eq. (41), with central difference quotients, a system of 3J+3 nonlinear equations for the 3J+3 unknowns (F_j^n, U_j^n, V_j^n) is obtained. The system can easily be solved by the block elimination after linearization by applying Newton's method. The pressure gradient appearing in eq. (40) was treated as a nonlinear eigenvalue. Details of the numerical method are found in [15].

The temperature distribution. The method used to obtain solutions of eq. (35) is similar to that described in the previous section.
Reducing eq. (35) to a first-order system of differential equations gives

$$P = \theta' \tag{43}$$

$$\left(b_2 P\right)' = Pr\left(U \frac{\partial \theta}{\partial \bar{z}} - P \frac{\partial F}{\partial \bar{z}}\right) \tag{44}$$

with the boundary conditions

$$\bar{y} = 0 \; : \; P = -1$$

$$\bar{y} = \bar{y}_L \; : \; P = -\frac{\sqrt{Re_R}}{2} Pr\, U \frac{\partial \theta}{\partial \bar{z}} \tag{45}$$

Eq. (43) was approximated by central-difference quotients and averages about the midpoint $(\bar{z}_n, \bar{y}_{j-\frac{1}{2}})$, while eq. (44) was centered about the midpoint $(\bar{z}_{n-\frac{1}{2}}, \bar{y}_{j-\frac{1}{2}})$ using the same net defined by eq. (42). The solution of the resulting linear system of equations was obtained by the same block elimination method used with the momentum equation.

The Nusselt number. The Nusselt number, based on the local difference between wall temperature and the fluid bulk temperature is defined by

$$Nu = \frac{2\,R\,\partial T/\partial r\big|_w}{T_w - T_m} \tag{46}$$

with the definition of the fluid bulk temperature for an incompressible fluid according to

$$T_m = \frac{\int_A v_z\,T\,dA}{\int_A v_z\,dA} \tag{47}$$

Inserting eq. (47) into eq. (46) results in the following expression for the Nusselt number

$$Nu = \frac{-Re_R}{\sqrt{Re_R}\int_0^{1} U\,\theta\,d\bar{y} - \frac{\sqrt{Re_R}\,\theta_w}{2}} \tag{48}$$

3. RESULTS AND DISCUSSION

3.1 Velocity Distribution

The effects of tube rotation on the axial velocity distribution in the rotational entrance region are shown in fig. 4 for various rotation rates N and different flow-rate Reynolds numbers. Experimental results of Reich [8] are plotted for comparison. Generally the calculated profiles of the axial velocity are in good agreement with experiments. However, the entrance velocity profile deviates from the experimental results. The experimental results show a more turbulent profile. We suppose, that either the entrance region of 40 pipe diameters was to short to produce a fully developed turbulent entrance velocity profile, or the mixing length hypothesis is in error for such low Reynolds numbers.
For increasing flow-rate Reynolds numbers ($Re_D = 20000$), where the entrance profile is in closer agreement with the data, the development of the axial velocity profile in the rotational entrance region is in excellent agreement with experimental findings.
The profiles shows, that there exists a potential core in the pipe, which is not affected by the tube rotation for low z/D. The velocity profiles adopt a flat shape near the center region for $z/D < 80$. The fluid in this region is only accelerated by tube rotation. For $z/D > 80$ the centrifugal forces influence the center region (fig. 2) and the shape of the profiles in the core region is altered by rotation. This typical development of the axial velocity profile was also mentioned by Nishibori et al. [16].

For the calculations of the velocity distributions and temperature profiles a strongly nonuniform grid with approximately 60 grid points in radial direction was used. It enables to predict the strong variations of velocity and temperature in the near wall region with good accuracy.

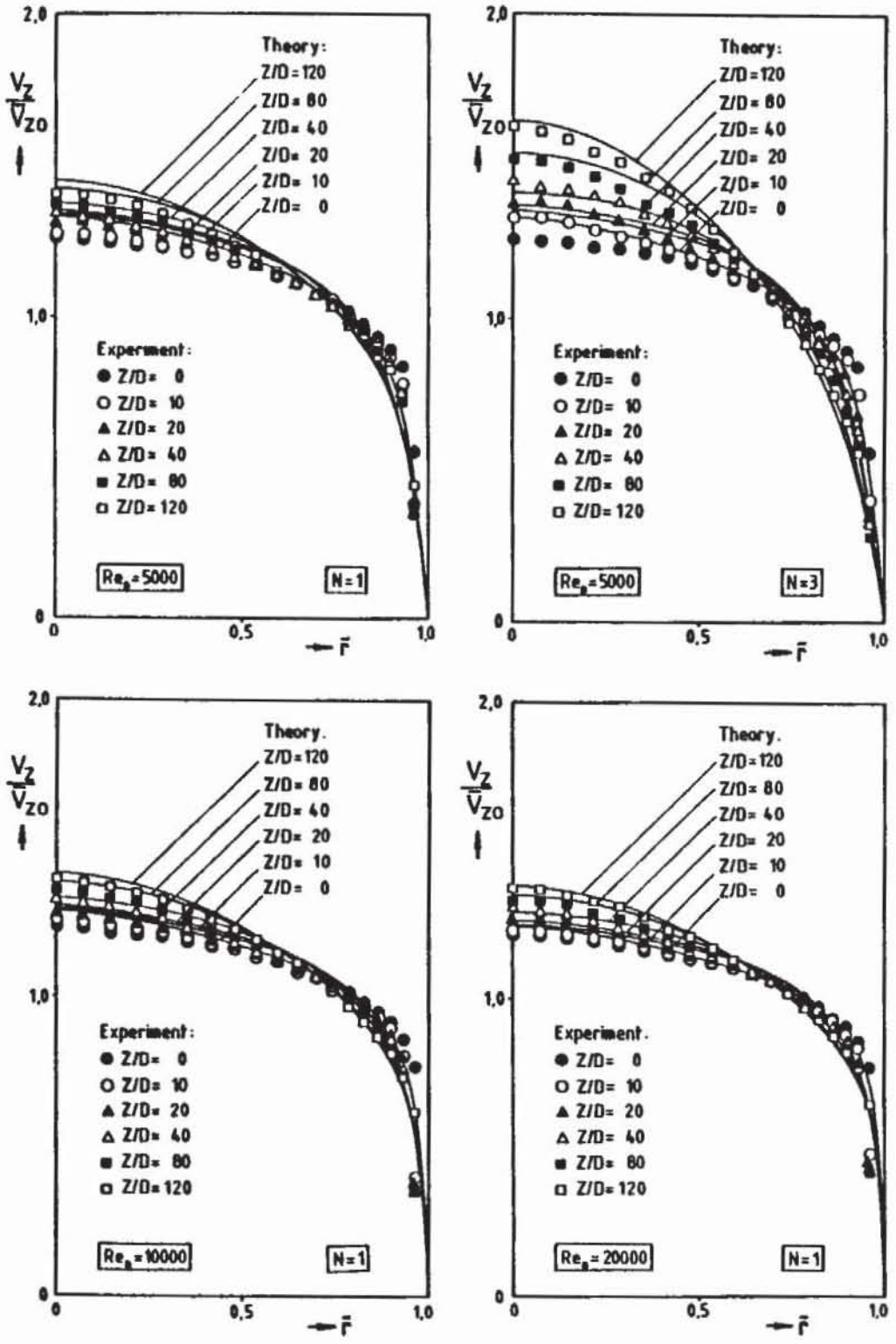

FIGURE 4. Axial velocity distribution as a function of z/D.

Fig. 5 shows fully developed velocity profiles for two flow-rate Reynolds numbers and different rotation rates N, compared with experimental results of [8]. This may be considered as an other proof for the validity of the applied method.

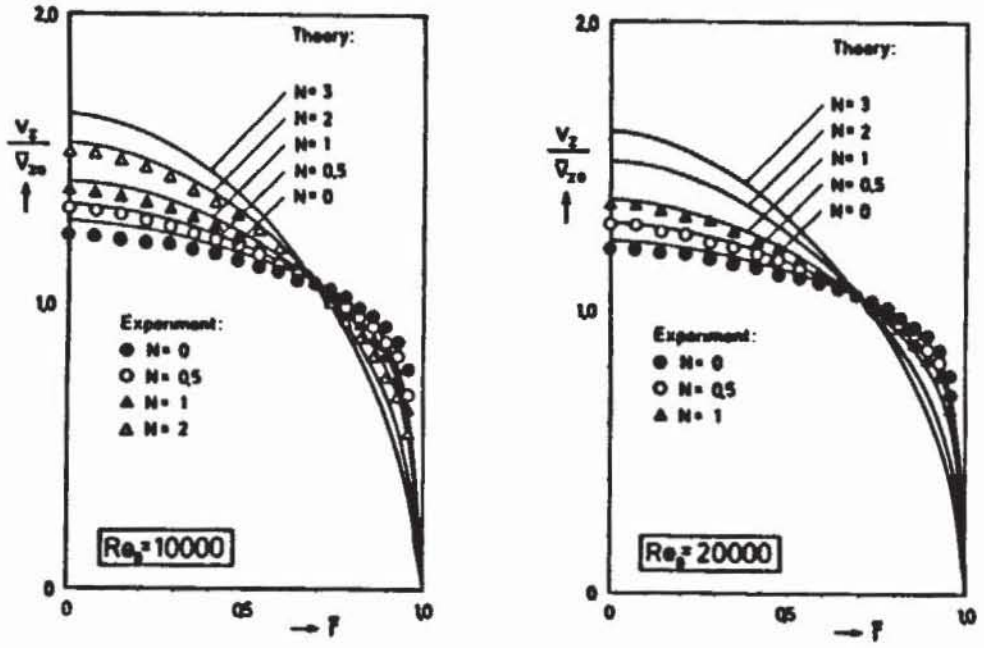

FIGURE 5. Axial velocity distribution for fully developed flow (z/D → ∞) as a function of the rotation rate N.

3.2 Richardson Number and Mixing Length

To illustrate the effect of turbulence suppression due to the pipe rotation in the rotational entrance, distributions of the Richardson number and the mixing length are depicted in fig. 6 and fig. 7 respectively, for various values of z/D.
With growing z/D the influence of the centrifugal forces expands increasingly across the cross section of the pipe. For z/D > 80 the whole cross section is seized by the radially growing centrifugal forces.
The development of the Richardson number explains the appearance of a

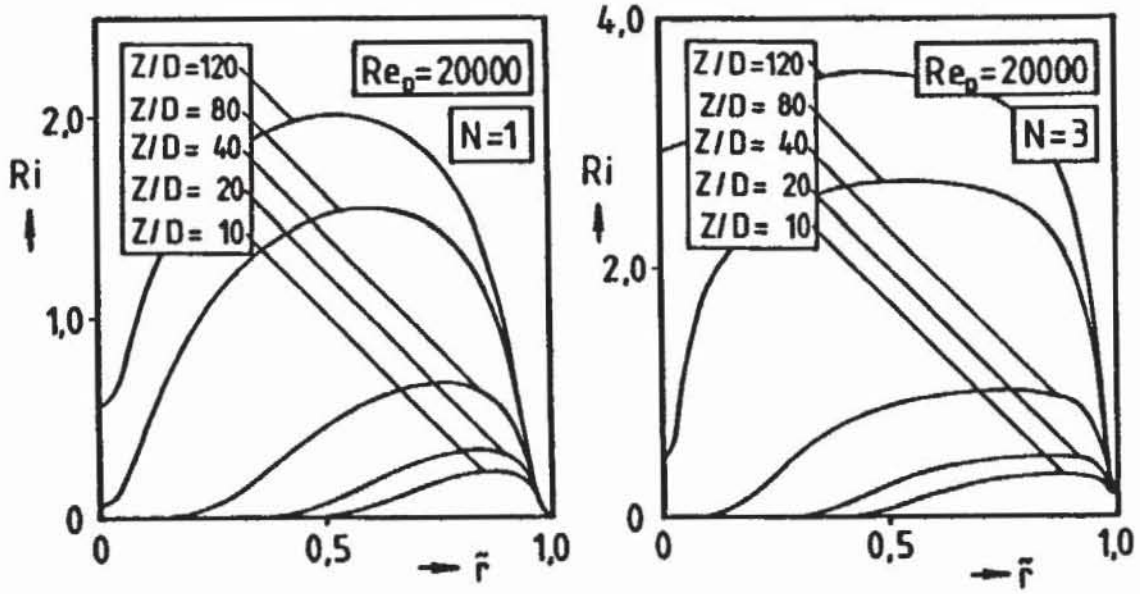

FIGURE 6. The Richardson number Ri for various z/D

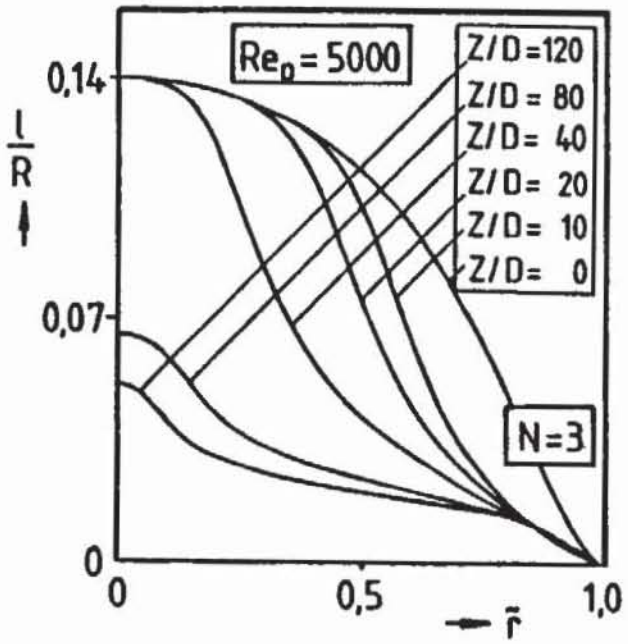

FIGURE 7. The mixing length l/R as a function of z/D.

potential core in the axial velocity, because in the region $0 < z/D < 80$ no suppression of turbulent fluctuations takes place near the pipe center and, therefore, a fully turbulent flow is established in this region. Because of laminarization of the flow close to the wall, the velocity gradient decreases at the wall and the central core is accelerated for reason of conservation of mass, eq. (36). Fig. 7 shows the influence of the tube rotation on the mixing length l for $Re_D = 5000$ and $N = 3$. For turbulent pipe flow ($z/D = 0$), the mixing length distribution is that one given by Nikuradse with the van Driest damping factor, eq. (18). The mixing length distribution, obtained from eq. (14), elucidates the turbulence suppression with increasing z/D.

3.3 The Nusselt Number

In fig. 8 the Nusselt number Nu_∞ for fully developed flow is plotted as a function of the flow-rate Reynolds number for various values of the rotation rate N and for Pr = 0.71. With increasing N a remarkable decrease in the Nusselt number can be observed. For $N \to \infty$ the Nusselt number approaches gradually the value for laminar pipe flow, which is $Nu_\infty = 4.36$ for constant heat flux at the wall.
Fig. 9 shows the local Nusselt number Nu for air (Pr = 0.71) devided by Nu_∞ for different flow-rate Reynolds numbers and various N. Because laminarization takes place, the flow is not fully developed for z/D = 120 and N = 3. This is a very interesting consequence of the laminarization phenomena. With increasing rotation rate N, the thermal entrance region is markedly enlarged, which was first recognized in [6]. For $N \to \infty$ the thermal entrance length L/D will approach $0.05\ Re_D Pr$, which is the entrance length for laminar pipe flow.

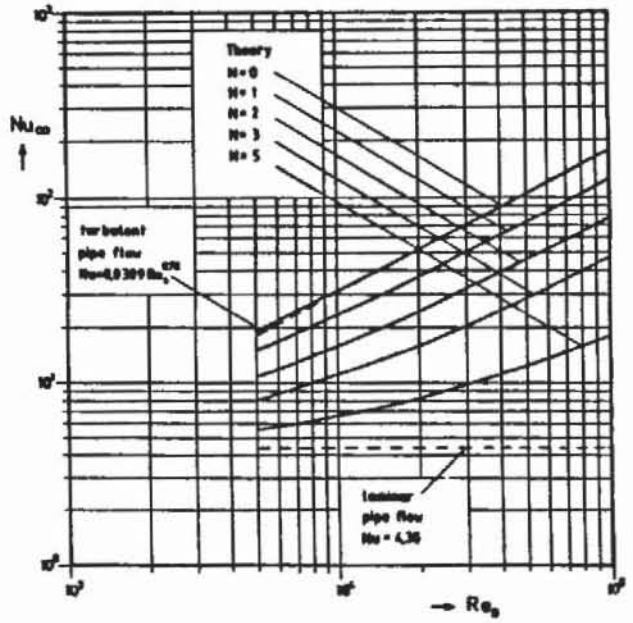

FIGURE 8. Nusselt number Nu_∞ for thermal and hydrodynamic fully developed flow as a function of Re_D with N as parameter (constant heat flux at the wall).

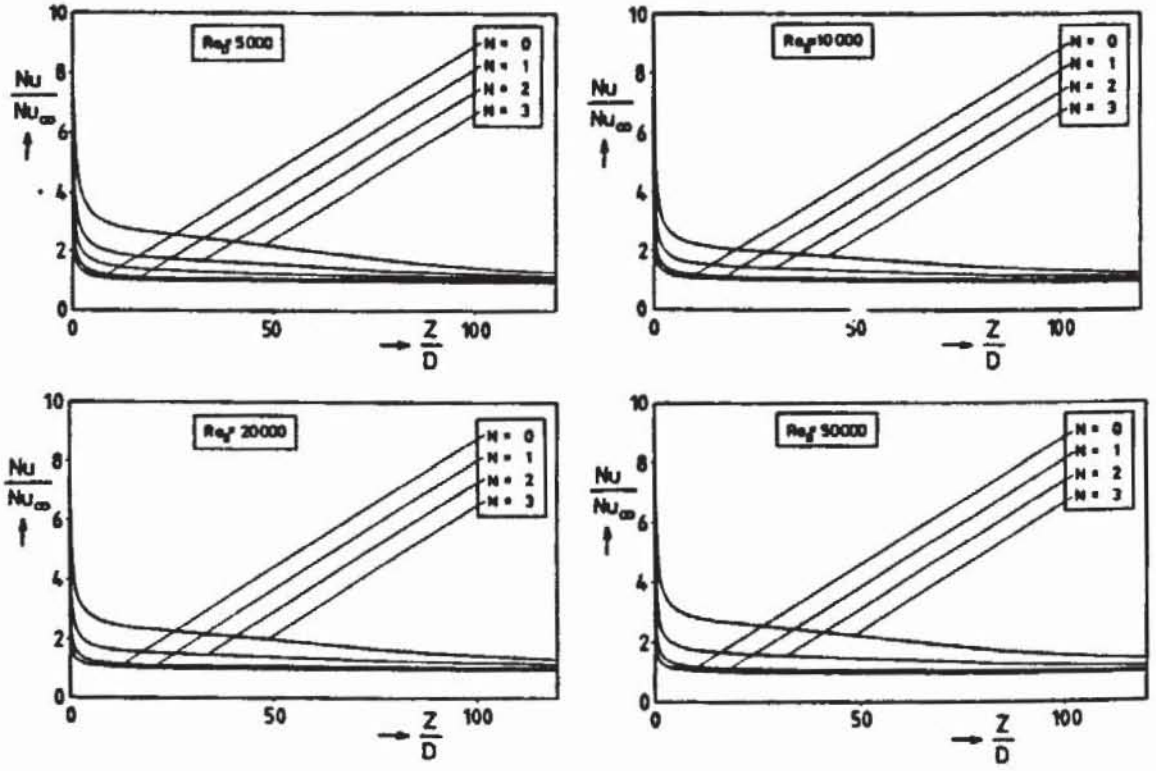

FIGURE 9. Nusselt number as a function of z/D with N as parameter (constant heat flux at the wall).

4. CONCLUSIONS

A theoretical model was presented to predict the complex interactions between turbulence suppression and tube rotation in the rotational entrance region of a pipe rotating about its axis. With the assumption of a quite universal tangential profile and the use of a modified mixing length hypothesis, which takes into account the turbulence suppression due to centrifugal forces, the axial velocity distribution and the Nusselt number were calculated. The theoretical results were verified by experimental findings [8] and a generally good agreement was found. It could be stated that tube rotation will enhance the thermal entrance length, because of flow laminarization.
An extrapolation to $N > 3$ is admissible only if future experimental results will confirm the universality of the tangential velocity profiles according to eq. (10.)

NOMENCLATURE

a	thermal diffusivity
c_p	specific heat at constant pressure
D	pipe diameter
F	stream-function
k	thermal conductivity
L	pipe length
l, l_q	hydrodynamic and thermal mixing length in the rotating pipe
l_o, l_{qo}	hydrodynamic and thermal mixing length in the nonrotating pipe
N	rotation rate
Nu	Nusselt number
Pr	Prandtl number
Pr_t	turbulent Prandtl number
p	pressure
$\dot{q}$	heat flux density
$\dot{q}_{rW}$	heat flux density at the pipe wall
R	pipe radius
Re	flow-rate Reynolds number
Re_φ	rotational Reynolds number
Ri	Richardson number
r	radial coordinate
T	temperature
T'	temperature fluctuation
T_m	bulk temperature
v_r, v_φ, v_z	time mean velocity in r, φ, z -direction
$v_{\varphi W}$	tangential velocity of the pipe wall
$\tilde{v}_r, \tilde{v}_\varphi, \tilde{v}_z$	dimensionless velocity components
$\bar{v}_{zo}$	mean axial velocity over the pipe cross section
v_i'	velocity fluctuation
$v_\star$	friction velocity
$y^+, \tilde{y}, \bar{y}$	dimensionless radial distance from the wall
z	axial coordinate
$\tilde{z}$, $\bar{z}$	dimensionless axial coordinate
ε_m^+	eddy diffusivity for momentum
θ	dimensionless temperature
μ	dynamic viscosity
ν	kinematic viscosity
τ_{ij}	shear stress
β	function according to eqs. (16) and (17)
ρ	density

REFERENCES

1. Levy F., Strömungserscheinungen in rotierenden Rohren, *VDI Forschungsarbeiten auf dem Gebiet des Ingenieurwesens*, vol. 322, pp. 18-45, 1929

2. Murakami, M., K. Kikuyama, Turbulent Flow in Axially Rotating Pipes, *J. of Fluid Engng.*, vol. 102, pp. 97 - 103, 1980.

3. Kikuyama K., M. Murakami, K. Nishibori, K. Maeda, Flow in an Axially Rotating Pipe, *Bull of the JSME*, vol. 26, pp. 506 - 513, 1983.

4. Bradshaw, P., The Analogy Between Streamline Curvature and Buoyancy in Turbulent Shear Flow, *J. of Fluid Mechanics*, vol 36, pp. 171 - 191 1969.

5. Reich, G., H. Beer, Fluid Flow and Heat Transfer in an axially rotating pipe, *The Second Int. Symp. on Transport Phenomena, Dynamics and Designe of Rotating Machinery*, vol. 1, pp. 298-313, 1988.

6. Weigand, B., H. Beer, Wärmeübertragung in einem axial rotierenden, durchströmten Rohr im Bereich des thermischen Einlaufs, *Wärme- und Stoffübertragung*, vol. 24, pp. 191-202, 1989.

7. Hennecke, D., Heat Transfer by Hagen-Poiseuille Flow in the thermal development region with axial conduction, *Wärme- und Stoffübertragung*, vol. 1, pp. 177 - 184, 1968.

8. Reich, G., Strömung und Wärmeübertragung in einem axial rotierenden Rohr, Doctoral Thesis, TH Darmstadt, 1988.

9. Kikuyama, K., M. Murakami, K. Nishibori, Development of Three-Dimensional Turbulent Boundary Layer in an Axially Rotating Pipe, *J. of Fluids Engng.*, vol. 105, pp. 154 - 160, 1983.

10. Koosinlin, M.L., B.E. Launder, B.I. Sharma, Prediction of Momentum, Heat and Mass Transfer in Swirling Turbulent Boundary Layers, *J. of Heat Transfer*, vol. 96, pp. 204 - 209, 1974.

11. Hirai, S., T. Takagi, M. Matsumoto, Predictions of the Laminarization Phenomena in an Axially Rotating Pipe Flow, *J. of Fluids Engng.*, vol. 110, pp. 424 - 430, 1988.

12. Schlichting, H., *Grenzschichttheorie*, 8d ed., Braun Karlsruhe, 1982.

13. Ludwieg, H., Bestimmung des Verhältnisses der Austauschkoeffizienten für Wärme und Impuls bei turbulenten Grenzschichten, *Z. für Flugwiss.*, vol. 4, pp. 73 -81, 1956.

14. Cebeci, T., K.C. Chang, A General Method For Calculating Momentum and Heat Transfer in Laminar and Turbulent Duct Flows, *Numerical Heat Transfer*, vol 1, pp. 39 - 68, 1978.

15. Cebeci, T., P. Bradshaw, Physical and Computational Aspects of Convective Heat Transfer, *Springer, New York*, 1984.

16. Nishibori, K., K. Kikuyama, M. Murakami, Laminarization of Turbulent Flow in the Inlet Region of an Axially Rotating Pipe, *Bull. of the JSME*, vol. 30, pp. 255-260, 1987.